Electronic Supplementary Material (ESI) for Physical Chemistry Chemical Physics.

Electronic Supplementary Information for:

Phase Stability of the Tin monochalcogenides SnS and SnSe: a Quasi-Harmonic Lattice-Dynamics Study

Ioanna Pallikara[a] and Jonathan M. Skelton[*a]

[1]*Department of Chemistry, University of Manchester, Oxford Road, Manchester M13 9PL, UK*

[*]*E-Mail: jonathan.skelton@manchester.ac.uk*

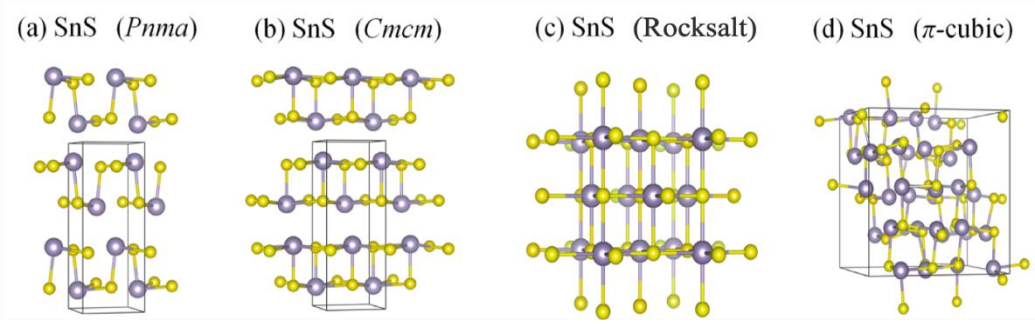

Figure S1. Optimised structures of *Pnma*, *Cmcm*, rocksalt and π-cubic SnS. These images were produced using the VESTA software.[1]

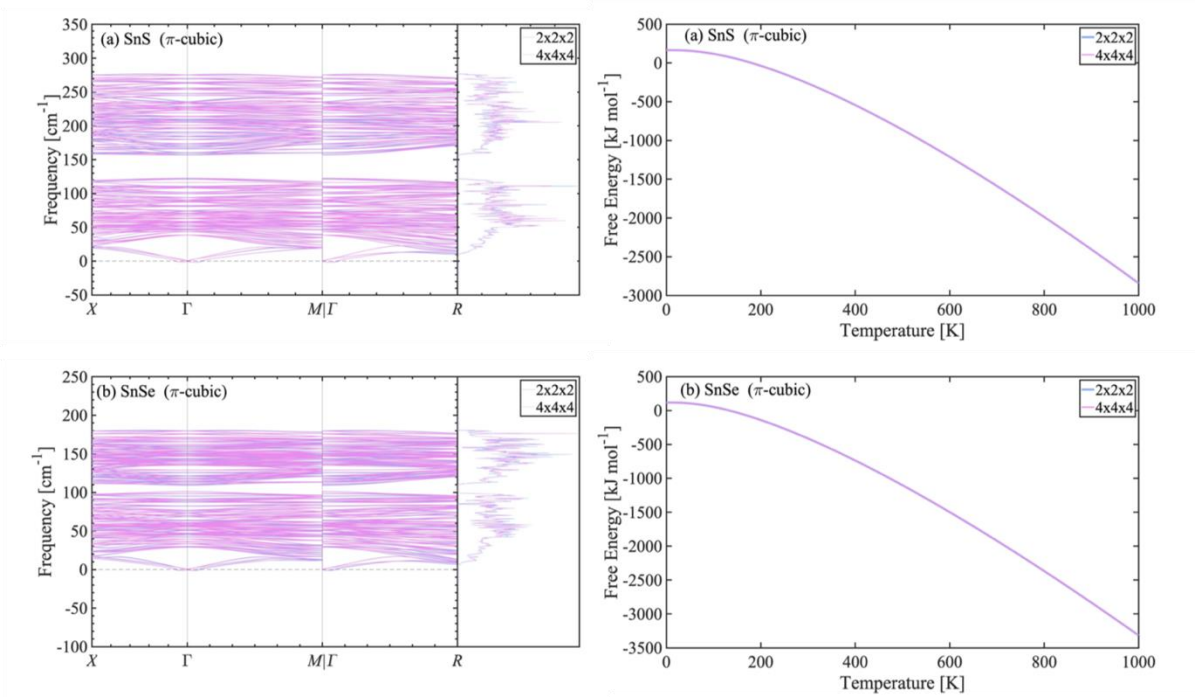

Figure S2. Phonon dispersion and density of states curves and vibrational Helmholtz free energy of the π-cubic phases of SnS (a) and SnSe (b) computed using two ***k***-point meshes with 2 × 2 × 2 and 4 × 4 × 4 subdivisions. Both calculations were performed on the equilibrium structure using the 64-atom unit cell, so the equivalent ***k***-point meshes for the 2 × 2 × 2 supercell used in the production calculations would be meshes with 1 × 1 × 1 (i.e. the Γ point) and 2 × 2 × 2 subdivisions.

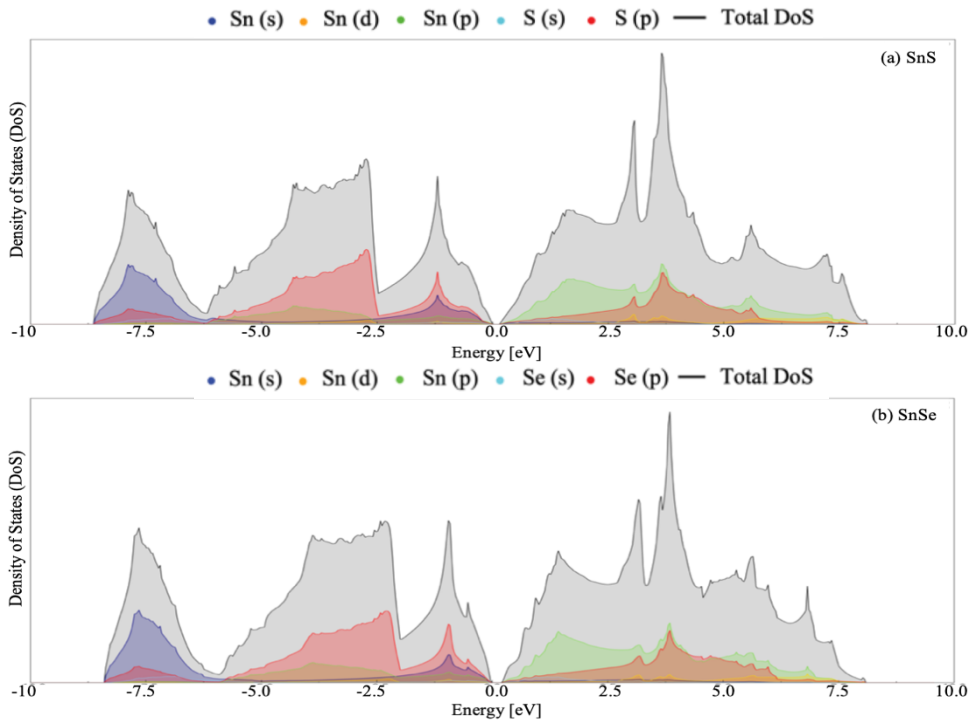

Figure S3. Calculated electronic atom- and orbital-projected density of states (DoS) curves for the rocksalt phases of (a) SnS and (b) SnSe. The states are colored as follows: Sn(s) - blue, Sn(d) - yellow, Sn(p) - green, S/Se(s) - cyan, S/Se(p) - red and total DoS - black.

Table S1. Calculated electronic bandgaps of the four phases of SnS (top) and SnSe (bottom) obtained using the PBEsol + D3 functional, with experimental and theoretical data for comparison where available.

Bandgaps: SnS [eV]			
Phase	PBEsol + D3 (this work)	Experiments	Other DFT studies
Rocksalt	0.15	-	0.52[2]
Pnma	0.579	1.33-1.6[3]	1.352[4],1.8[5]
Cmcm	0.549	-	1.4[5]
π-cubic	1.13 (indirect)	1.53[6]	1.74[7]
Bandgaps: SnSe [eV]			
Phase	PBEsol + D3 (this work)	Experiments	Other DFT studies
Rocksalt	0.253	-	0.58[2]
Pnma	0.423	0.89[8], 1.0-1.2[9]	0.79[10], 1.18,[4] 0.4[11]
Cmcm	0.234	0.39[8]	0.05[11]
π-cubic	0.856 (indirect)	1.28[12]	0.799/1.011 (LDA/GGA)[13]

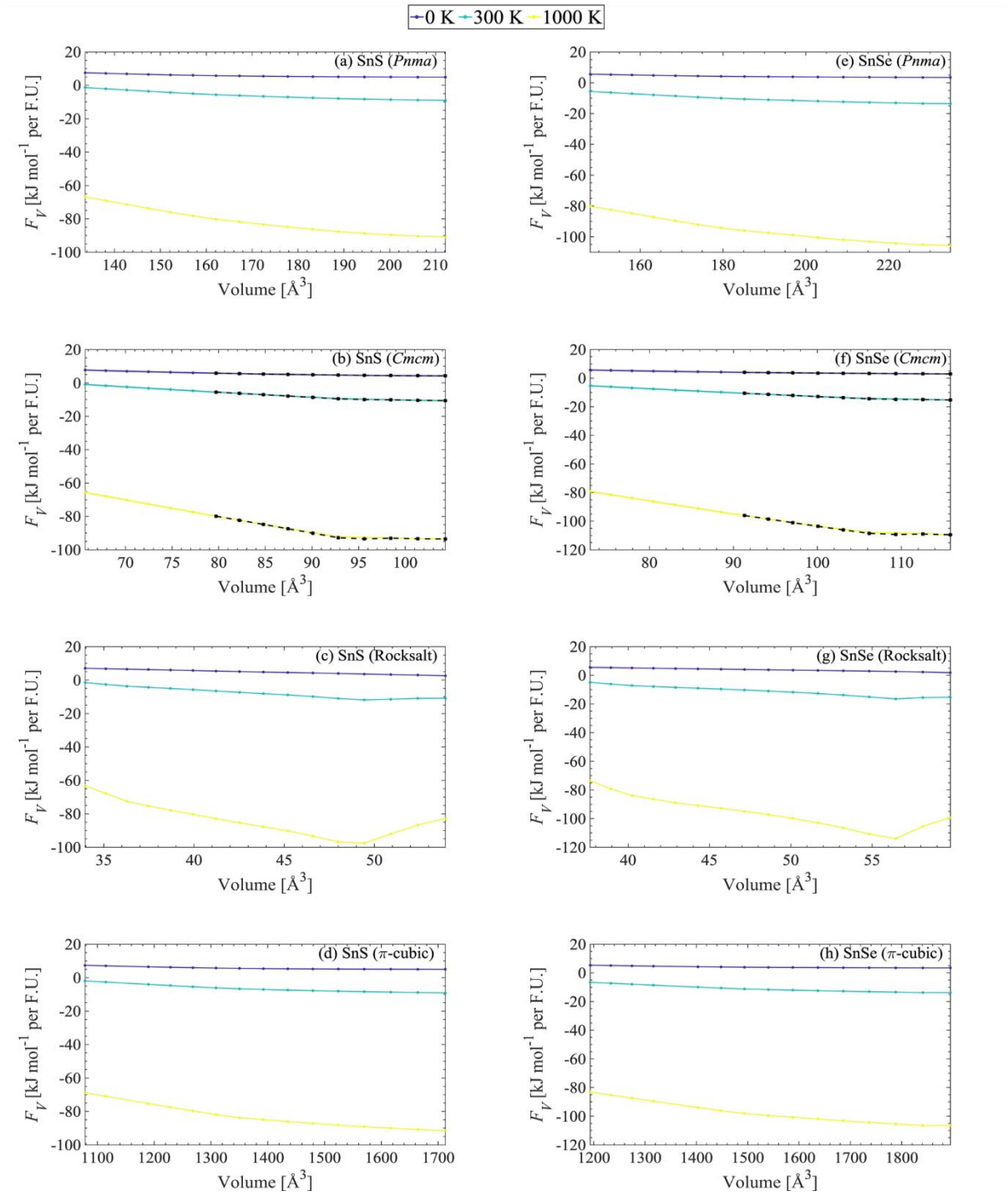

Figure S4 Phonon free energy F_V as a function of volume for the eight tin monochalcogenide phases examined in this work at T = 0, 300 and 1000 K. For the *Cmcm* phases in (b) and (f), the data overlaid in black shows the F_V obtained after renormalisation of the principal imaginary modes at the Γ and Y wavevectors.

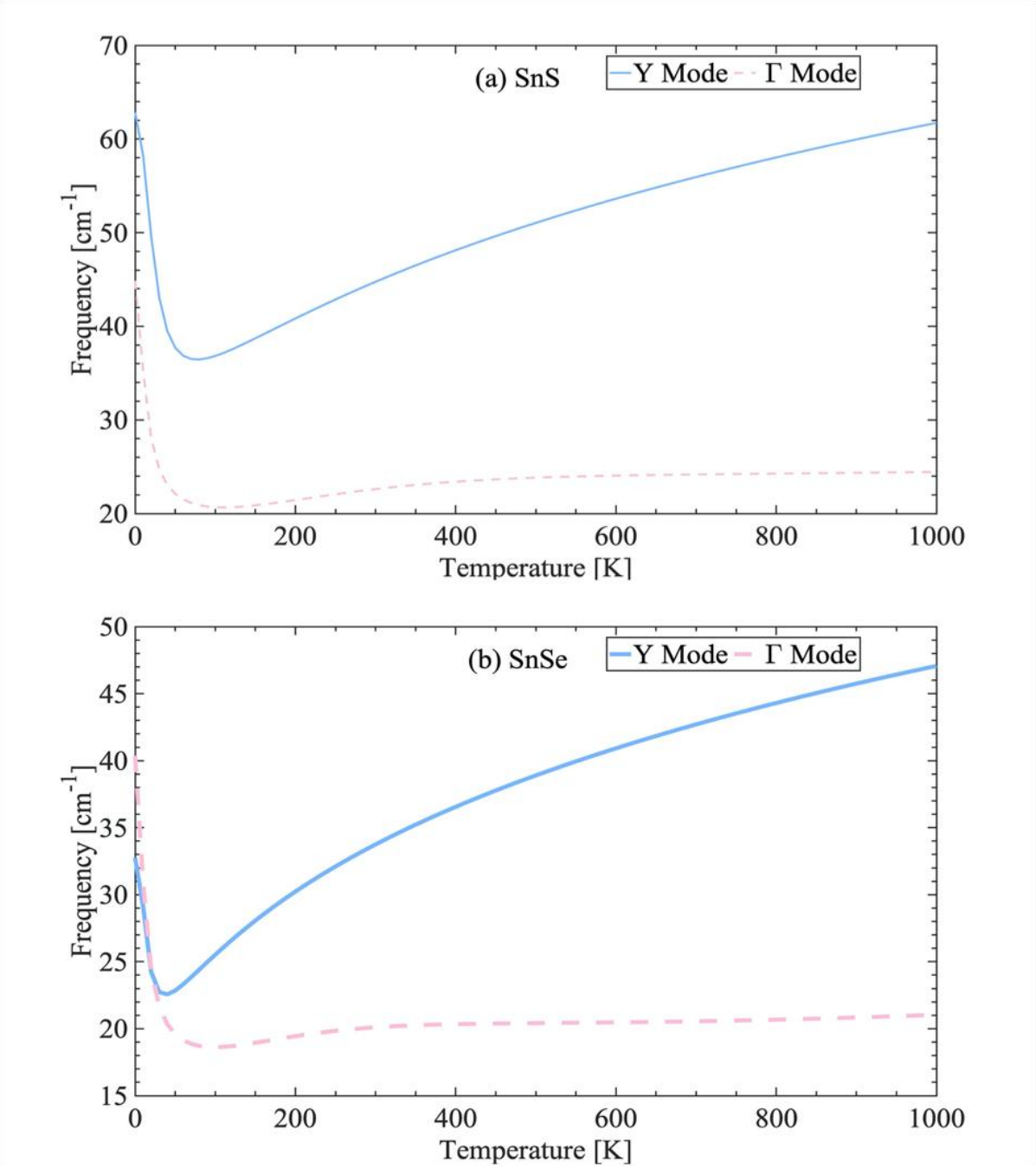

Figure S5. Effective renormalised frequencies of the two imaginary modes of *Cmcm* SnS (a) and SnSe (b) at the equilibrium volume, as a function of temperature, obtained using the method in Ref. 14.

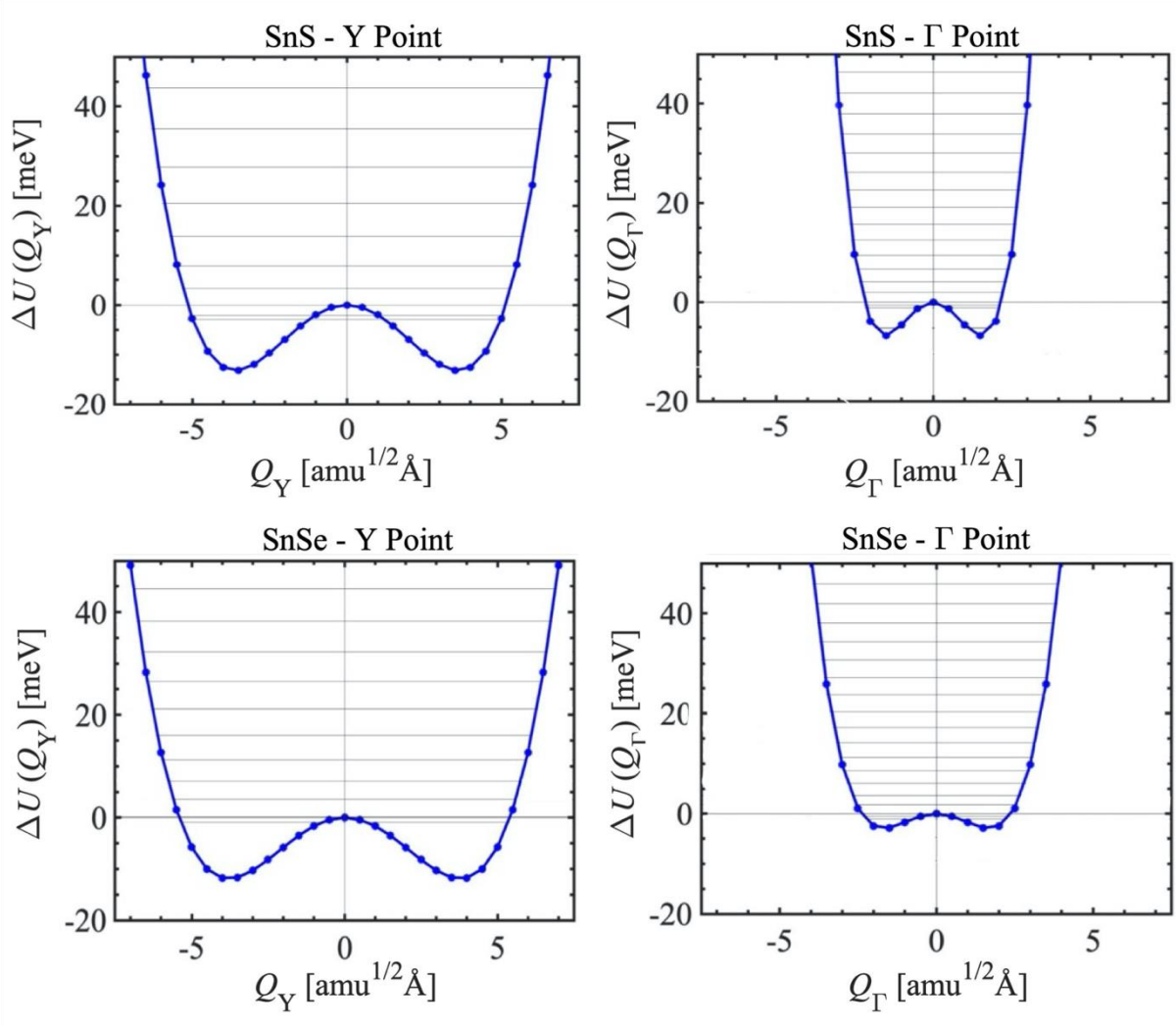

Figure S6. Anharmonic double-well potentials along the two principal imaginary modes at the Y and Γ wavevectors of *Cmcm* SnS (top) and SnSe (bottom) at the equilibrium volume. The black lines inside the potentials show the eigenvalues obtained by solving a 1D Schrödinger equation for the potential.

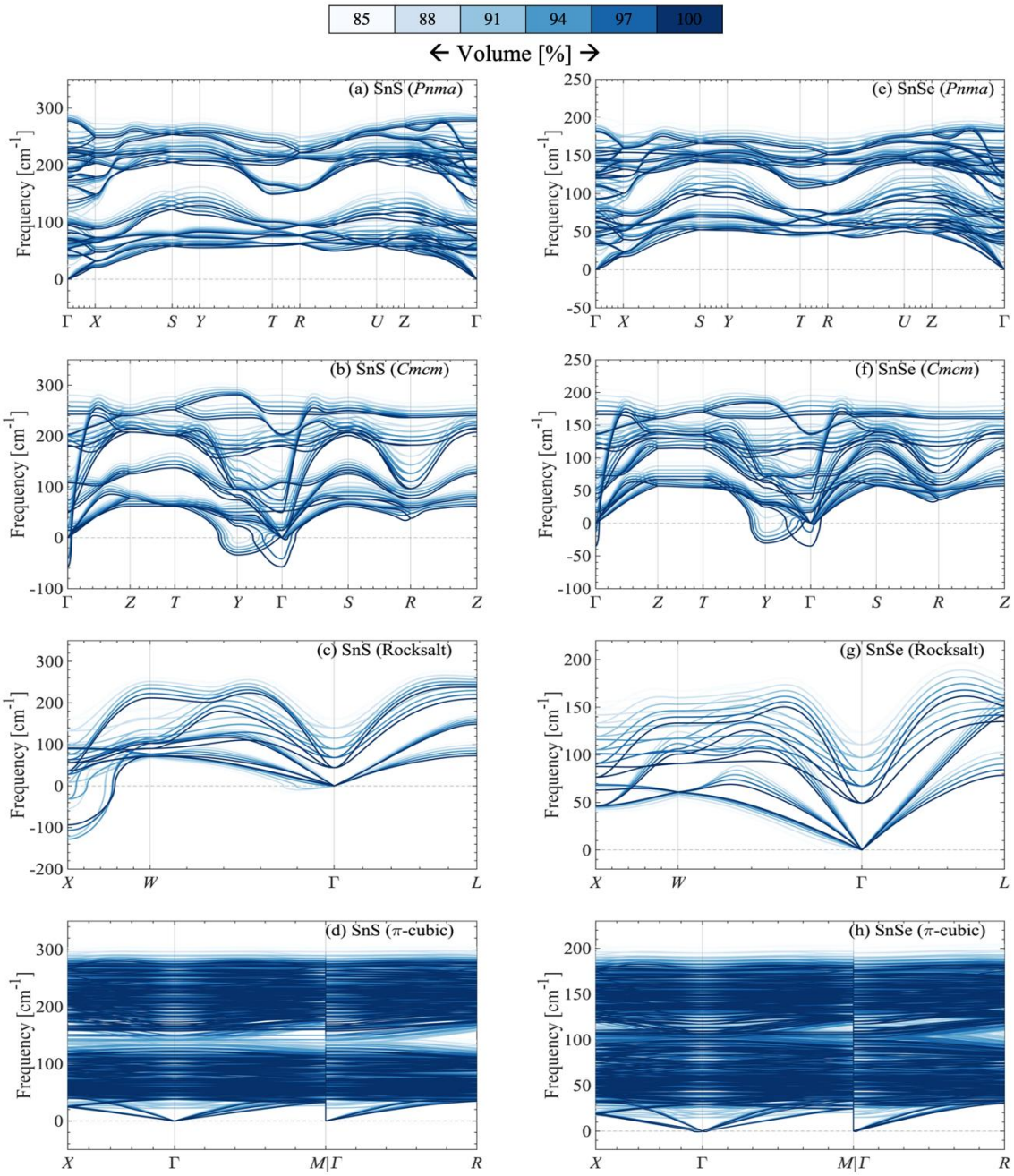

Figure S7. Phonon dispersion and density of states curves for SnS ((a)-(d), left) and SnSe ((e)-(h), right) under up to 15 % volume compression: (a)/(e) *Pnma*, (b)/(f) *Cmcm,* (c)/(g) rocksalt and (d)/(h) π-cubic.

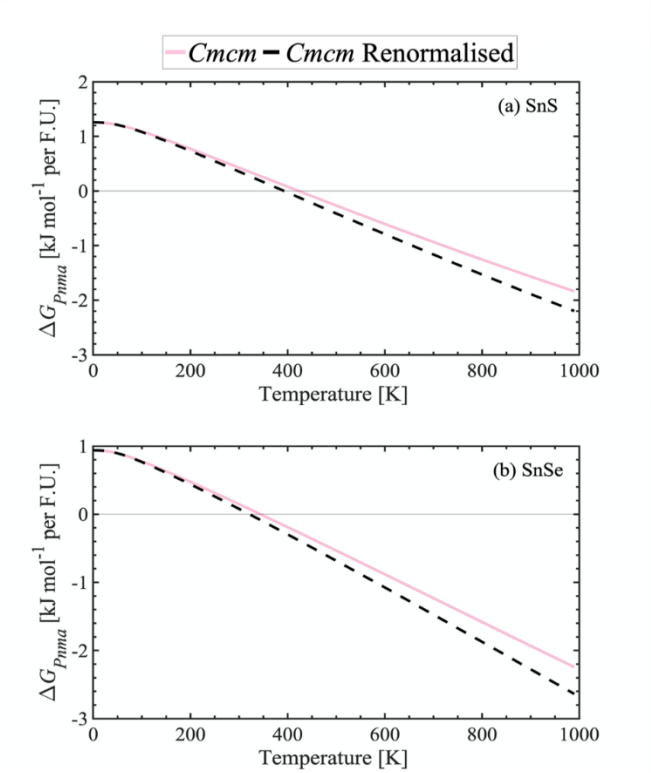

Figure S8. Gibbs energy differences ΔG_{Pnma} between the *Pnma* and *Cmcm* phases of (a) SnS and (b) SnSe before (pink) and after renormalization of the imaginary harmonic modes (black).

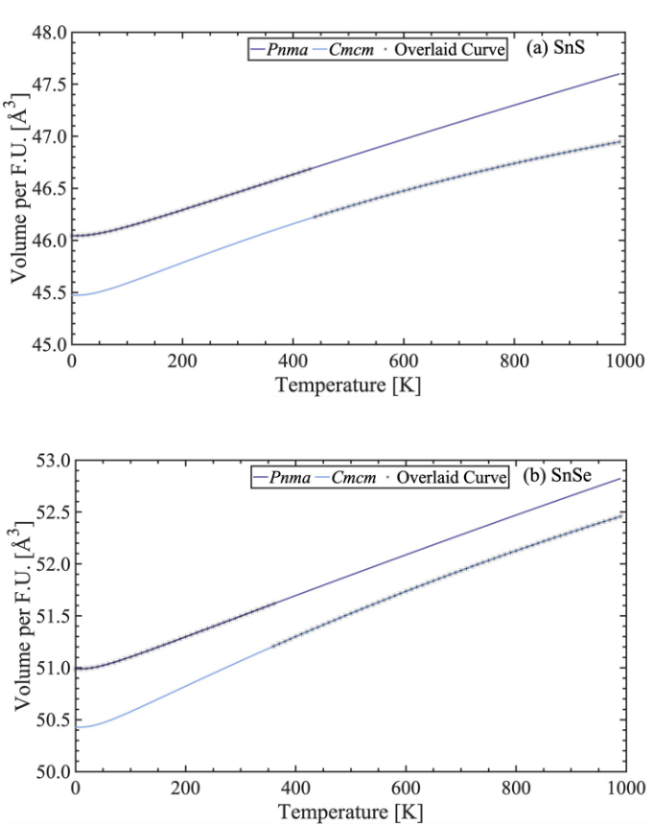

Figure S9. Calculated volume per formula unit as a function of temperature for the *Pnma* (purple) and *Cmcm* (light blue) phases of (a) SnS and (b) SnSe. The black stars track the volumes of the phases with the lowest-energy Gibbs free energy to highlight expected discontinuities in the volume at the phase transition.

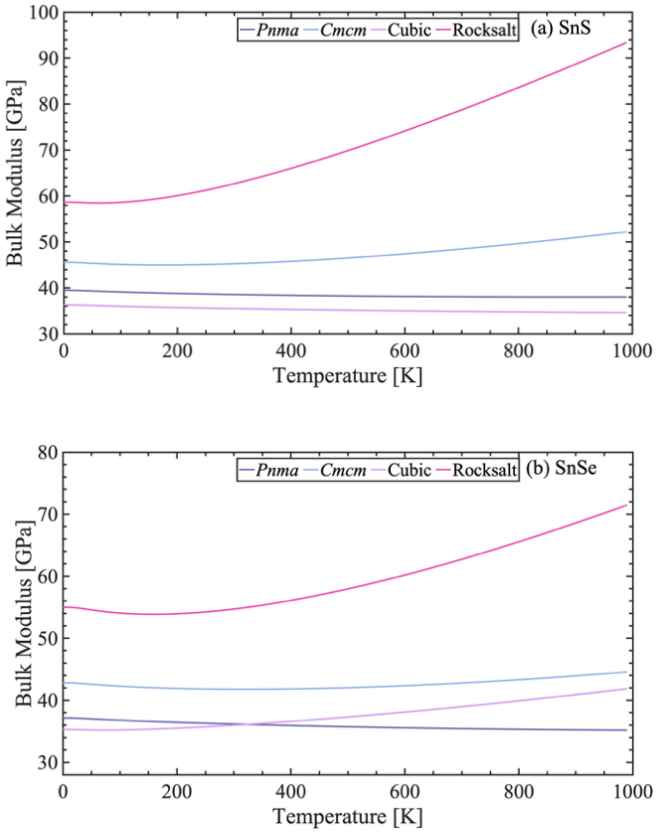

Figure S10. Calculated bulk modulus as a function of temperature for the *Pnma* (purple), *Cmcm* (light blue), π-cubic (purple) and rocksalt (pink) phases (a) SnS and (b) SnSe.

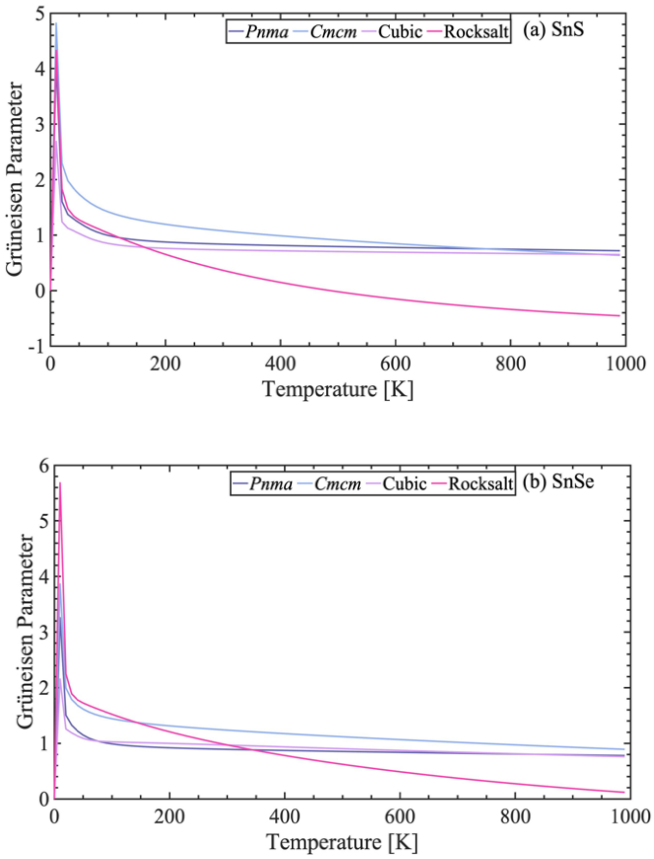

Figure S11. Calculated Grüneisen parameter as a function of temperature for the *Pnma* (purple), *Cmcm* (light blue), π-cubic (purple) and rocksalt (pink) phases (a) SnS and (b) SnSe.

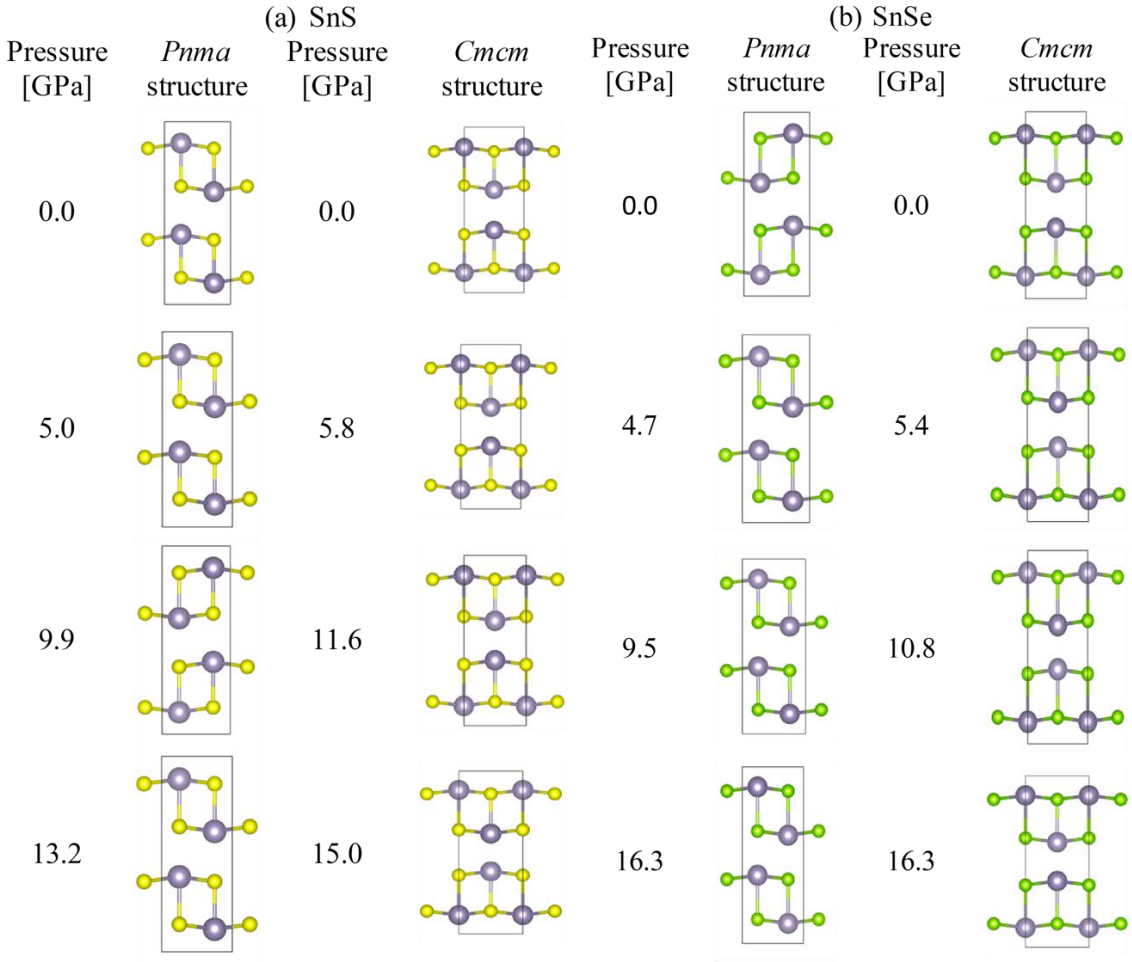

Figure S12. Optimized structures of *Pnma* and *Cmcm* SnS (a) and SnSe (b) at a range of applied pressures. The images were produced using the VESTA software.[1]

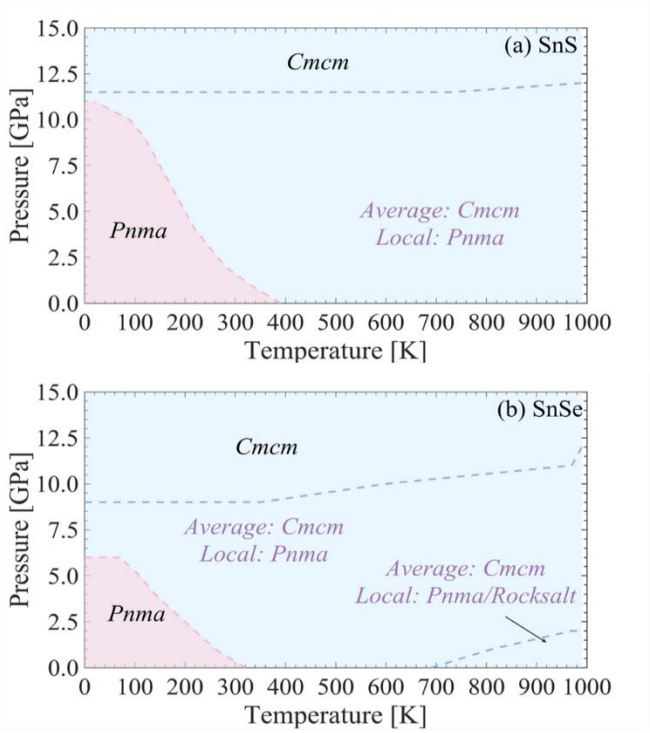

Figure S13 Calculated temperature-pressure phase diagrams of (a) SnS and (b) SnSe, obtained based on the Gibbs energies calculated within the quasi-harmonic after renormalization of the imaginary harmonic modes in the *Cmcm* phases. This may be compared with Fig. 9 in the text.

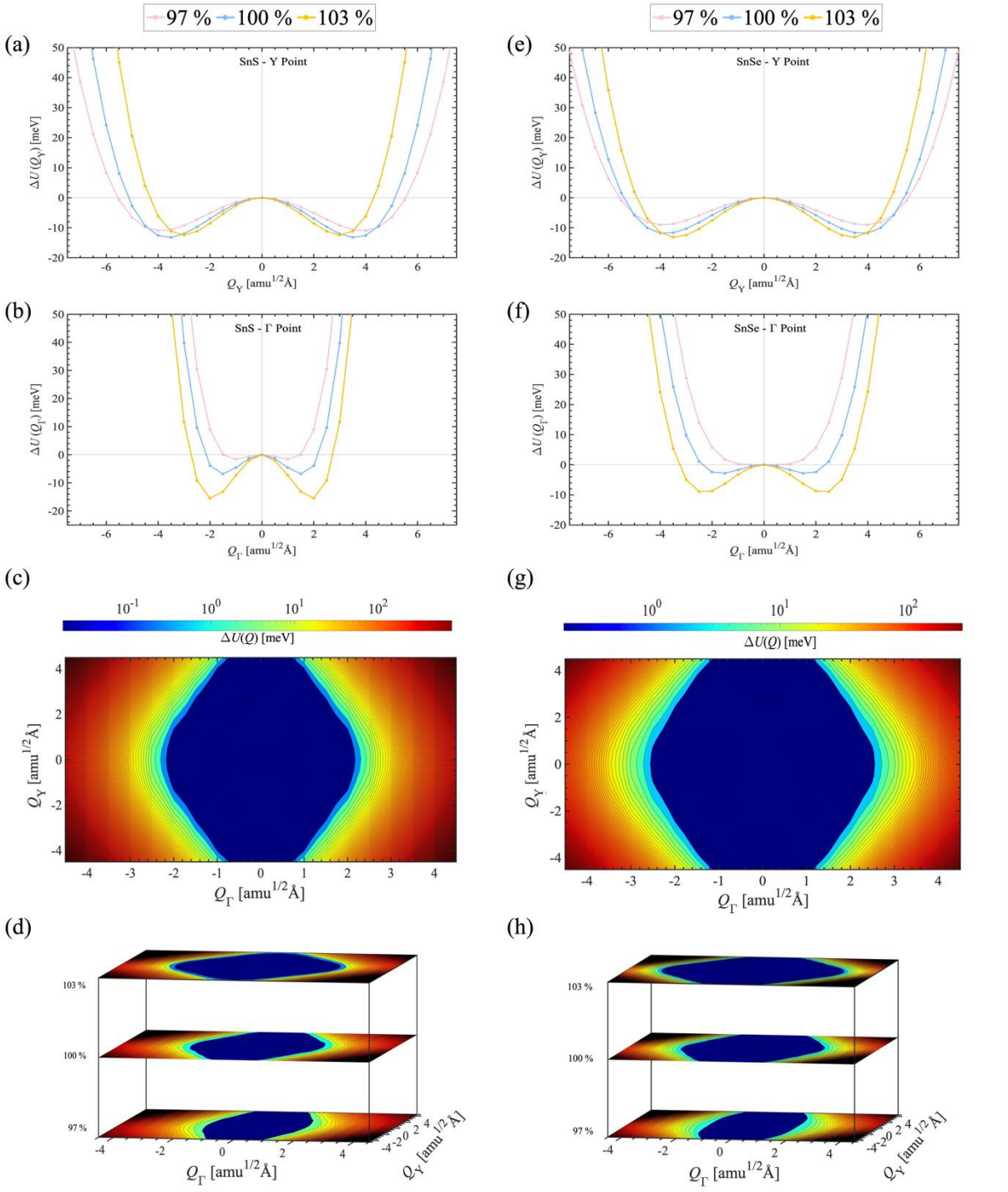

Figure S14. Potential-energy surface (PES) along the two principal imaginary modes at the Y- and Γ wavevectors in *Cmcm* SnS (a)/(b) and SnSe (e)/(f), evaluated at the equilibrium volume and 3 % expansions and compressions. (c)/(g) Two-dimensional PES spanned by both imaginary modes at the equilibrium volumes for (c) SnS and (g) SnSe. (d)/(h) Comparison of the 2D PES for the three volumes shown in (a)/(b) and (e)/(f).

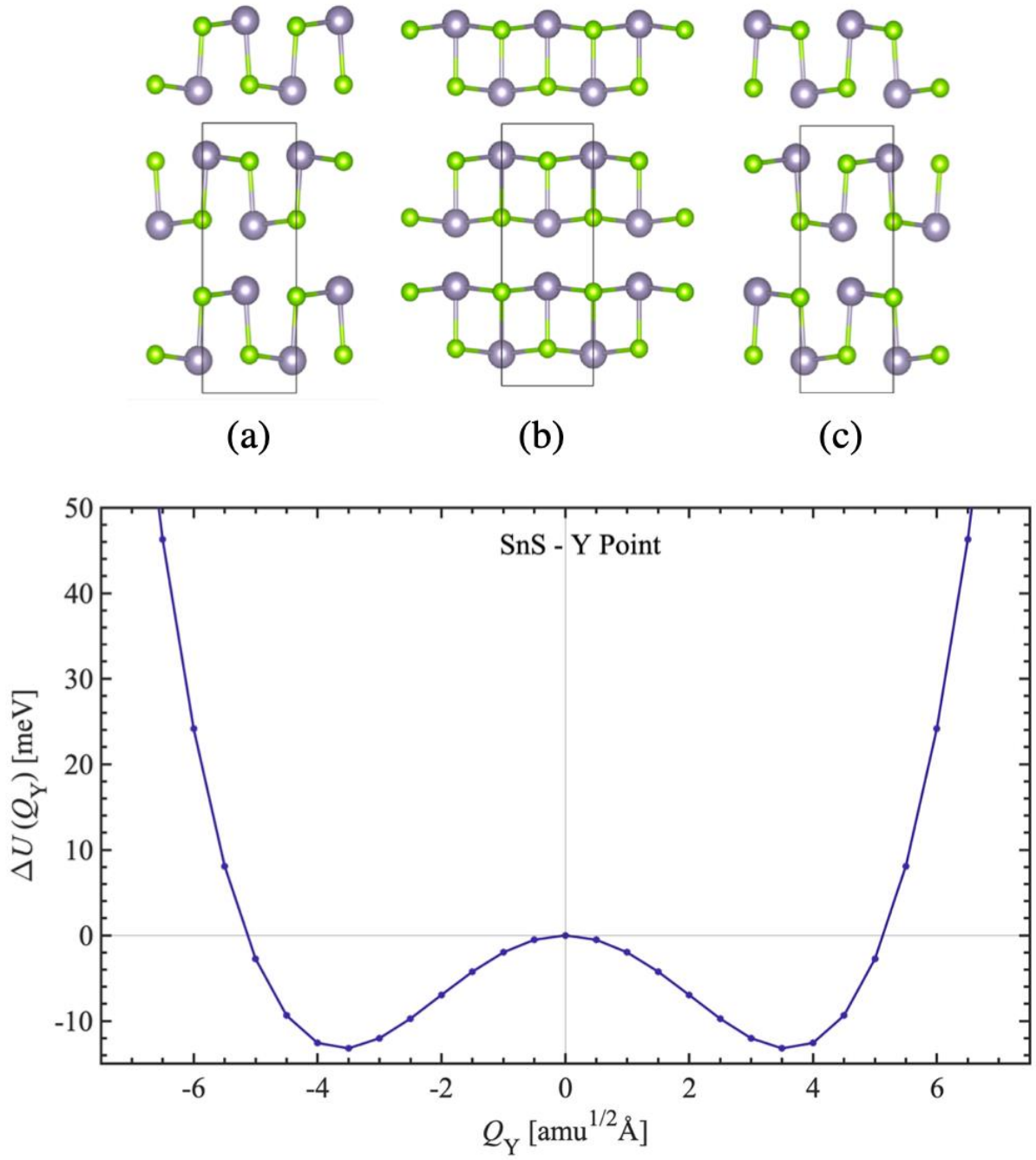

Figure S15. Structures of SnS associated with the minima in the 1D potential-energy surface (PES) obtained by mapping the Y-point imaginary mode in the equilibrium structure. (a) Minimum at Q = -3.5 amu$^{1/2}$ Å. (b) Maximum at Q = 0. (c) Minimum at Q = +3.5amu$^{1/2}$ Å. (a) and (c) correspond to the distorted *Pnma* phase, while (b) corresponds to the *Cmcm* average structure.

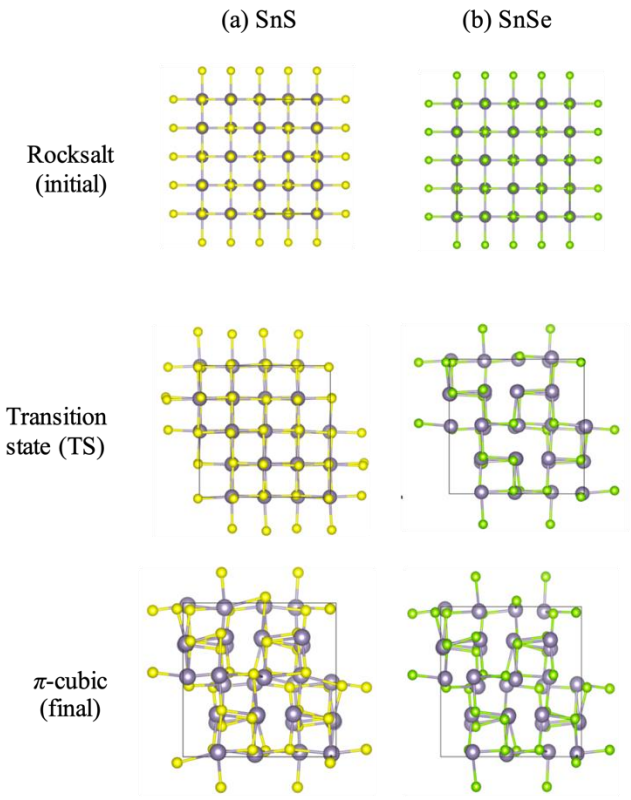

Figure S16. Structures of the initial (rocksalt), transition state (TS), and final (π-cubic) structures of SnS (a) and SnSe (b) obtained from the climbing image nudged elastic band (CI-NEB) calculations. These images were produced by the VESTA software.[1]

References

1 K. Momma and F. Izumi, *J. Appl. Crystallogr.*, 2011, **44**, 1272–1276.

2 Y. Sun, Z. Zhong, T. Shirakawa, C. Franchini, D. Li, Y. Li, S. Yunoki and X. Q. Chen, *Phys. Rev. B - Condens. Matter Mater. Phys.*, 2013, **88**, 235122–235122.

3 G. Valiukonis, D. A. Guseinova, G. Krivaite and A. Sileika, *Phys. Status Solidi*, 1986, **135**, 299–307.

4 A. Walsh and G. W. Watson, *J. Phys. Chem. B*, 2005, **109**, 18868–18875.

5 N. Koteeswara Reddy, M. Devika and E. S. R. Gopal, *Crit. Rev. Solid State Mater. Sci.*, 2015, **40**, 359–398.

6 R. E. Abutbul, E. Segev, L. Zeiri, V. Ezersky, G. Makov and Y. Golan, *RSC Adv.*, 2016, **6**, 5848–5855.

7 J. M. Skelton, L. A. Burton, F. Oba and A. Walsh, *APL Mater.*, 2016, **5**, 036101.

8 L. D. Zhao, S. H. Lo, Y. Zhang, H. Sun, G. Tan, C. Uher, C. Wolverton, V. P. Dravid and M. G. Kanatzidis, *Nature*, 2014, **508**, 373–377.

9 F. D. Murnaghan, *Proc. Natl. Acad. Sci. U.S.A.*, 1944, **30**, 244–247.

10 L. T. Yang, L. P. Ding, P. Shao, Y. H. Tiandong, Z. L. Zhao, F. H. Zhang and C. Lu, *J. Alloys Compd.*, 2021, **853**, 157362.

11 Y. Lu, F. W. Zheng, Y. Yang, P. Zhang and D. B. Zhang, *Phys. Rev. B*, 2019, **100**, 054304.

12 R. E. Abutbul, E. Segev, S. Samuha, L. Zeiri, V. Ezersky, G. Makov and Y. Golan, *CrystEngComm*, 2016, **18**, 1918–1923.

13 S. U. Rehman, F. K. Butt, F. Hayat, B. Ul Haq, Z. Tariq, F. Aleem and C. Li, *J. Alloys Compd.*, 2018, **733**, 22–32.

14 J. M. Skelton, L. A. Burton, S. C. Parker, A. Walsh, C.-E. Kim, A. Soon, J. Buckeridge, A. A. Sokol, C. R. A. Catlow, A. Togo and I. Tanaka, *Phys. Rev. Lett.*, 2016, **117**, 075502.